DOI: https://doi.org/10.37434/tpwj2026.08.01

# FEATURES OF FORMATION OF THE STRUCTURE AND BALLISTIC RESISTANCE OF ARMOR STEEL WELDED JOINTS PRODUCED BY PULSED PLASMA ARC WELDING WITH COMBINED ALLOYING OF THE WELD METAL

**O.A. Slyvinskyy[1,2], V.D. Poznyakov[2], V.M. Korzhyk[2], Ye.V. Illiashenko[2], S.P. Bisyk[3]**

[1]National Technical University of Ukraine "Igor Sikorsky Kyiv Polytechnic Institute"
37 Prosp. Beresteiskyi, 03056, Kyiv, Ukraine
[2]E.O. Paton Electric Welding Institute of the NASU
11 Kazymyr Malevych Str., 03150, Kyiv, Ukraine
[3]National Defence University of Ukraine
28 Prosp. Povitrianykh Syl, 03049, Kyiv, Ukraine

**ABSTRACT**

The results of a study on the effect of pulsed-plasma welding with combined alloying of the weld metal using an austenitic filler wire and an insert rod on the structure formation and ballistic resistance of welded joints of modern high-hardness armor steels Armox 500T and Mars 600 are presented. It was established that pulsed-plasma welding ensures the formation of full-penetration butt joints with a thickness of 5–6 mm without edge preparation at a specific heat input of $Q/\delta \approx 0{,}16$ kJ·mm$^{-2}$. It is shown that at the same level of thermal input, welded joints of Mars 600 steel are characterized by a smaller width of the softened subzone within the heat-affected zone compared to Armox 500T steel, due to the increased resistance of the silicon-alloyed initial martensitic structure to short-term tempering. It was established that the combined alloying of the weld metal with OK Autrod 16.95 filler wire and OK Tigrod 308L insert rod, combined with a high proportion of the base metal in the weld formation, ensures the creation of high-strength martensitic-type structures. In the welded joints of Armox 500T steel, a martensitic-bainitic structure of the weld metal is formed, with a hardness that is not inferior to the hardness of the base metal. For Mars 600 steel, the formation of a heterogeneous martensitic structure of varying dispersion along the weld height was observed. In the upper part of the weld, a refined structure with signs of structureless martensite was detected. Based on the results of EDX and NDIR analysis, an uneven distribution of carbon and alloying elements along the weld height was established. The possible influence of the pulsating constricted plasma arc on the intensification of mass transfer and mixing of the weld pool metal is discussed, which may be one of the factors contributing to the formation of the observed structural anisotropy of the weld metal. Ballistic testing confirmed that the developed technology of pulsed-plasma welding with combined alloying of the weld metal ensures producing the welded joints of armor steels of various hardness classes with ballistic resistance equivalent to that of the base metal.

**KEYWORDS:** high hardness armor steel, pulsed plasma arc welding, combined alloying of the weld metal, structure formation, martensitic structures, heat-affected zone, ballistic resistance

## INTRODUCTION

Rolled sheets 2 to 20 mm thick from armor steels heat-treated to a high hardness of *HBW* 4.9–5.9 GPa are widely used for manufacture of the military and special equipment structures with armor protection from small arms bullets, as well as fragments of shells and mines. At present mechanized consumable electrode gas-shielded welding in active shielding gas (MAG) with application of high-alloyed Cr–Ni–Mn welding wires of austenitic class is the most common method of joining these materials in production [1]. Under the condition of minimal degree of mixing of the deposited and base metal the weld forms an austenitic or austenitic-ferritic structure, ensuring the required level of fatigue strength [2] and cold cracking resistance [3] of the welded joints. At the same time, a disadvantage of such a technological solution is a significant structural and mechanical mismatch between the metal of the weld, heat-affected zone (HAZ) and base metal of the armor. In particular, a microhardness gradient on the line of fusion of the weld and the HAZ overheated region is equal to 3.5–4.5 GPa·mm$^{-1}$ on average [4, 5]. Compared to the base metal, which usually has a homogeneous structure of fine-acicular tempered martensite, the metal of the austenitic weld has considerably lower values of dynamic strength and hardness, and is inferior to it by the ballistic resistance values [6].

One of the promising ways of solving this problem is controlled formation of the structural-phase composition of the weld metal due to an increase of the proportion of base metal in its composition and controlling the conditions of crystallization and phase transformations [7].

The previous research shows the possibility of increasing the hardness of armor steel weld metal by applying TIG-welding [8], hybrid laser-arc [9] and hybrid plasma-arc process [10, 11]. Promising is the application of pulsed-plasma welding, which combines the high energy concentration of the plasma arc with the possibility of independent adjustment of the heat input and quantity of filler metal. Such features of the process create the prerequisites for a controlled influence on the proportion of the base metal in the weld, intensification of mixing of the weld pool metal and formation of structures with higher strength and ductility values. Here, pulsation of current of the constricted plasma arc affects not only the thermal regime of the process, but also the hydrodynamic condition of the weld pool. The periodical change in current is accompanied by a change in the current density, degree of arc constriction, plasma flux velocity and its pressure on the melt surface. It results in enhancement of the convective flux mass transfer into the weld pool, which promotes more intensive mixing of the base and filler metals [12–16].

This is of particular importance for armor steel joints, as increase of the base metal proportion in the weld promotes the preservation of a sufficient carbon content in it for formation of martensitic-type structures. Moreover, intensification of mixing creates the preconditions for a more uniform distribution of alloying elements in the weld metal and a controlled formation of its structural-phase state [14–16].

In [5] it was found that the pulsed-plasma welding of armor steels allows an essential reduction of filler metal losses, compared to MAG welding, which promotes formation of a predominantly martensitic structure in the weld metal with hardness close to or even higher than that of the base metal. Owing to the features of low-temperature transformation of austenite a favourable residual stressed state is ensured in the weld metal that increases the cold cracking resistance of the joints [5].

At the same time, there are practically no data in the available literature as to the influence of such structural changes on the ballistic resistance of armor steel welded joints. The features of structure formation and weld metal ballistic resistance in case of simultaneous application of several high-alloy welding consumables and the influence of the pulsating plasma arc on the mass transfer and structure formation processes, remain particularly insufficiently studied.

## THE AIM

of the work is to establish the regularities of formation of the structure, hardness, and ballistic resistance of the welded joints of armor steels for ballistic protection, which were produced by pulsed-plasma welding with combined alloying of the weld metal by filler and insert welding consumables of austenitic class.

## MATERIAL AND METHODS OF INVESTIGATION

Investigations were conducted using rolled sheets from steels of two grades: Armox 500T and Mars 600. By its chemical composition (Table 1) and mechanical properties the rolled sheets from Armox 500T steel correspond to US DOD standard for high hardness armor (~500 *HB*) [17], and that from Mars 600 steel — to ultra-high hardness armor (~600 *HB*) [18].

Automatic pulsed-plasma welding was performed using PLAZER-300 EMF unit (Manufacturer "SCIENCE-PRODUCTION CENTER "PLAZER", Ukraine, TU U 27.9-38388946-001:2025). Butt joints of plates from Armox 500T steel 5.4 mm thick, from Mars 600 steel — 6.2 mm thick, without edge preparation were produced on a copper backing with a machined backing groove. Plasma-forming gas Ar and shielding gas — a mixture of Ar + 18 % $CO_2$ — were applied. Results of works [19–22] were used during selection of the optimal welding modes.

A feature of the welding technology was simultaneous application of two welding consumables of different brands (Table 1). ESAB OK Autrod 16.95 filler wire 1.0 mm in diameter was used. In addition to it, an ESAB OK Tigrod 308L insert rod 1.2 mm in diameter was placed in the gap between the plates to be welded during welding of Mars 600 steel and a rod 1.0 mm in diameter was used for welding Armox 500T steel plates, in order to control the structural-phase composition of the weld. The rod was located at ~1.0 mm distance from the lower plane of the plates being joined.

The welding mode parameters (Table 2) were selected in order to ensure a complete penetration of the joints in one pass, with simultaneous minimizing of the heat input into the base metal: $I_{av}$ — average value of modulated current, applied for energy input calculation; $I_p$ and

**Table 1.** Chemical composition of the base materials and welding consumables, wt.%

| Material | C | S | P | Si | Mn | Ni | Cr | Mo | B | Al |
|---|---|---|---|---|---|---|---|---|---|---|
| Base material | | | | | | | | | | |
| Armox 500T | 0.28 | 0.002 | 0.007 | 0.24 | 0.85 | 0.90 | 0.50 | 0.354 | 0.001 | 0.050 |
| Mars 600 | 0.43 | 0.0006 | 0.0054 | 0.82 | 0.499 | 1.881 | 0.15 | 0.33 | 0.0028 | 0.035 |
| Welding consumables | | | | | | | | | | |
| OK Autrod 16.95 | 0.06 | 0.010 | 0.020 | 0.80 | 6.70 | 8.10 | 18.2 | 0.10 | – | – |
| OK Tigrod 308L | 0.018 | 0.007 | 0.018 | 0.33 | 2.0 | 10.3 | 20.0 | 0.11 | – | – |

**Table 2.** Parameters of the modes of experimental sample welding

| Sample material | $I_{av}$, A | $I_p$, A | $I_{paus}$, A | $f$, Hz | $S$ | $U_w$, V | $V_f$, m/min | $V_w$, mm/s | $Q$, kJ·mm$^{-1}$ |
|---|---|---|---|---|---|---|---|---|---|
| Mars 600 | 213 | 290 | 180 | 300 | 3.3 | 26.0 | 1.9 | 3.3 | 1.0 |
| Armox 500T | 201 | 280 | 170 | 300 | 3.3 | 25.7 | 1.6 | 3.6 | 0.86 |

$I_{paus}$ — pulse and pause current; $f$ and $S$ — pulse frequency and duty cycle; $U_w$ — average value of welding current; $v_f$ and $v_w$ — filler wire feed rate and welding speed. Energy input $Q$ was calculated for the value of effective heating efficiency of plasma welding η = 0.6 according to DSTU ISO/TR 17671-1:2015.

Microstructure of the welded joints was studied in a metallographic microscope iScope IS.1053-PLMi (etchants: 4 and 15 % solution of nitric acid in ethyl alcohol to reveal the structure of the base metal and weld metal, accordingly) and in a scanning electron microscope TESCAN VEGA 3.

Vickers durometric test was conducted in microhardness meter LHVS-1000Z with the load of 2.94 N (300 g) in the welded joint cross-section in two measurement directions (Figure 1): at the depth of 1.5 mm from the face plane of the joined plates (direction $x$), as well as by the weld height — along their vertical axis (direction $y$).

Analysis of the chemical composition of the welds was conducted by the method of energy-dispersive X-ray (EDX) spectroscopy by mapping the surfaces of metallographic sections of 1×1 mm area and non-dispersion infrared-absorption (NDIR) spectroscopy using Horiba EMIA PRO detector.

Ballistic tests were conducted at the accredited Research Center for Testing, Expertise, and Certification of Personal Armored Protection Equipment of the National University of Defence of Ukraine to verify the compliance of welded samples with the protection class according to DSTU 3975-2000 "Armour Protection of Specialized Cars. General Technical Requirements". "The shooting was carried out from a distance of 10 m at an impact angle of 90° with 5.45 mm caliber bullets (5.45×39 assault rifle cartridge) of two types: PS with a core made of 65G steel heat-treated to a hardness of 56–60 *HRC*, and PP (improved penetration) with a conical core made of steel 75 with a hardness of 60 *HRC*.

## EXPERIMENTAL RESULTS

Within the HAZ of the studied welded joints, the results of microdurometric analysis (Figure 2) demonstrate a pattern of a change in hardness with greater distance from the weld, which is typical for welding the quenched and tempered steels, in particular armor steels.

Metal of the overheated complete recrystallization sections (HAZ1), which underwent austenitization during heating, after cooling has the maximal hardness, which is higher than that of the base metal (declared by manufacturers of both the steels minimal guaranteed base metal hardness in the heat-treated state is marked by horizontal dashed lines). Within the incomplete recrystallization and tempering regions (HAZ2), the hardness drop below the level of the base metal hardness values occurs as a result of the processes of tempering and recrystallization of the initial structure which are due to the influence of the welding heat. At the same time, microhardness distribution within the welds in the horizontal ($x$) and vertical ($y$) measurement directions is indicative of formation of high-hardness structures of the order of HAZ1 metal hardness.

Comparison of the results of durometric analysis of welded samples of Armox 500T and Mars 600

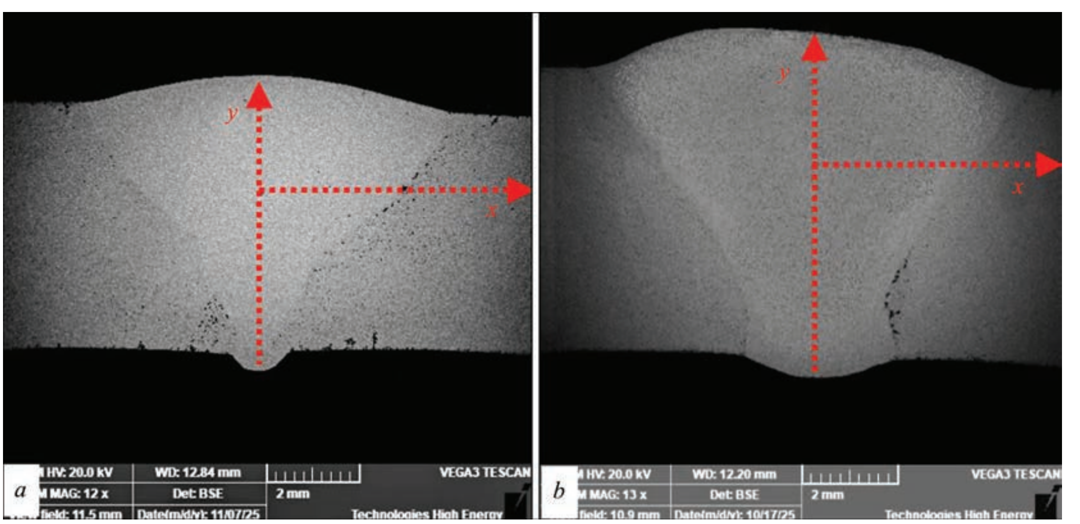


**Figure 1.** Shape of penetration of armor steel welded joints with marked directions of microhardness measurement: *a* — Armox 500T steel; *b* — Mars 600 steel

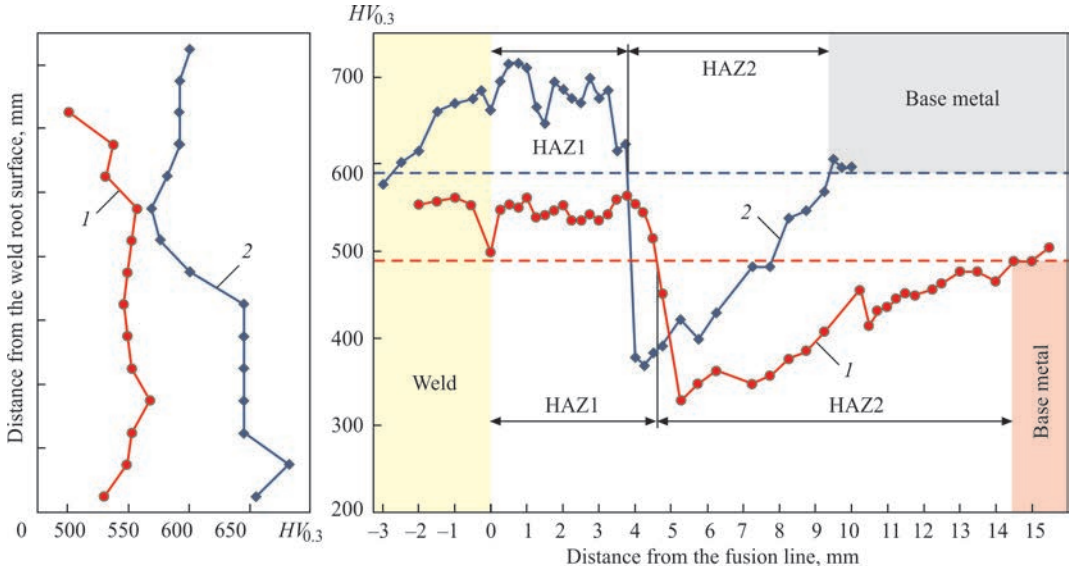


**Figure 2.** Microhardness distribution along the vertical axes of the welds and in the cross-section of the welded joints: *1* — Armox 500T steel; *2* — Mars 600 steel

steels shows that the extent of the HAZ in the joint of Armox 500T steel turned out to be markedly greater, first of all, due to its wider softened HAZ2 region. In the sample from Armox 500T steel in the vertical ($y$) measurement direction a noticeable microhardness reduction in the upper quarter of the weld is also observed, which is due to an increase in the deposited metal proportion in it. Microhardness distribution by the height of the weld formed during welding of a sample from Mars 600 steel allows outlining three regions: 1) near the weld root, ~3 mm high, with the highest hardness; 2) middle one, ~2 mm high, within which a gradual hardness reduction takes place; 3) upper one, ~2 mm high, with an intermediate microhardness value, compared to the two other regions.

Considering that for joints of both the steels the values of specific heat input are practically the same: $Q/\delta \approx 0.16$ kJ·mm$^{-2}$ (where $\delta$ is the base metal thickness), as well as due to the remoteness of the softened HAZ2 regions from the area of the metallurgical reactions with the welding consumables, the causes for greater extent of the HAZ in the welded joint of Armox 500T steel can only be attributed to differences in alloying and technologies of thermomechanical treatment of the studied steels. Metallographic studies of the base metal microstructure demonstrated the troostite-martensitic structure of the sample from Armox 500T steel (Figure 3, *a*), whereas Mars 600 steel has the structure of fine-acicular lath martensite (Figure 3, *b*). It is also worth noting the presence of bands with different etchability across the thickness of the rolled stock of both the steels. By the data of [23] for rolled steel armor Armox 500T these features of the structure state are associated not with the chemical heterogeneity of the material, but with the biomodal nature of distribution of the size of primary austenite grains formed during hot rolling. Higher etchability bands coincide with the location of fine grains of former austenite, and they look darker than the light-coloured bands of metal with coarser primary grain.

Comparison of chemical composition of the studied steels (Table 1) shows that while in Armox 500T silicon is a deoxidizer, Mars 600 steel is alloyed with this element. Considering that silicon in the martensite solid

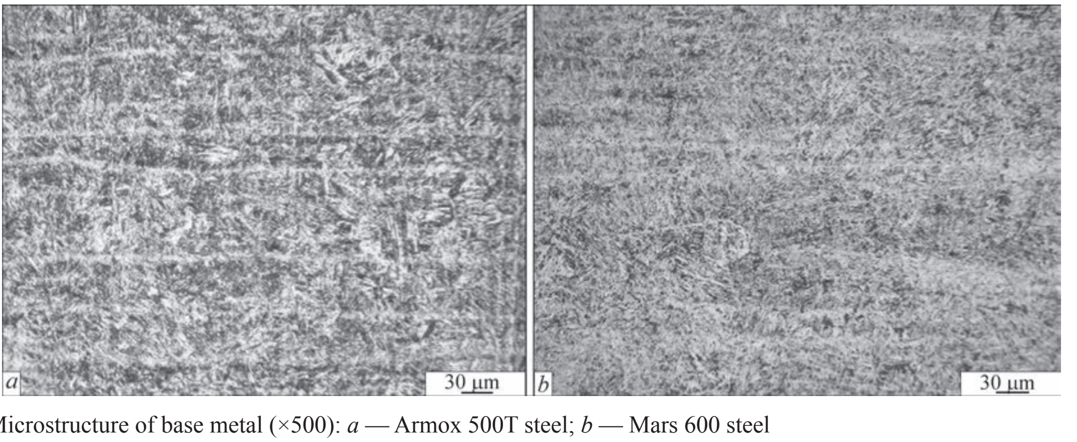


**Figure 3.** Microstructure of base metal (×500): *a* — Armox 500T steel; *b* — Mars 600 steel

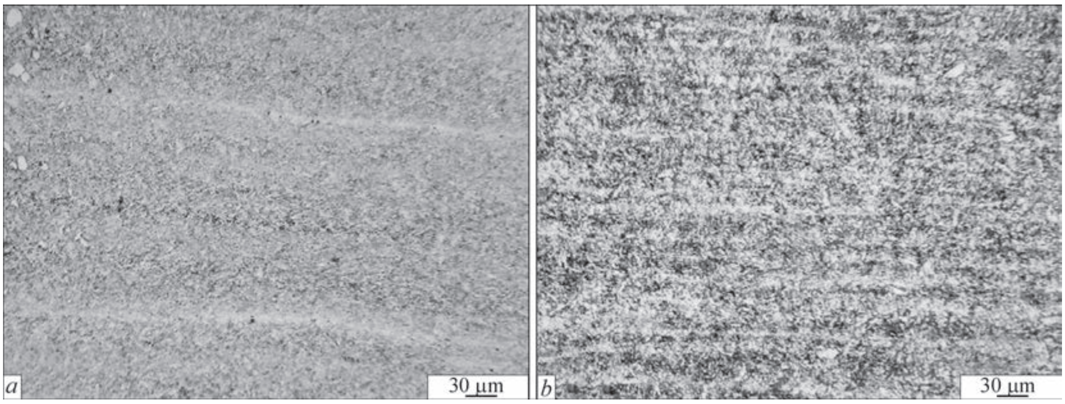

**Figure 4.** Microstructure of the high-tempered HAZ region (×500): *a* — Armox 500T steel; *b* — Mars 600 steel

solution slows down the diffusion mobility of carbon in the crystalline lattice, and inhibits carbide nucleation at the initial tempering stages [24, 25], short-term heating of the welding HAZ portion of Mars 600 steel, the most remote from the weld, to low-tempering temperatures did not lead to any significant changes in its structural state or hardness. As a result, the width of the softened region (HAZ2) of the welded sample of this steel turned out to be smaller, and the visible changes in its structure compared to the base metal were observed only for the metal which was heated to the high-tempering temperatures. Figure 4 is a comparison of the microstructure in high-tempered regions of the HAZ of the produced welded joints. In the Armox 500T steel sample the primary structure bimodal in terms of the primary grain size distribution was transformed into tempered troostite along the higher etchability band and recrystallized granular ferrite along the light etching bands (Figure 4, *a*). The metal structure in the high-tempered region of the sample from Mars 600 steel is more homogeneous and it consists of just tempered troostite (Figure 4, *b*).

Metallographic investigations of the welded sample from Armox 500T steel did not reveal any noticeable differences in the microstructure in different weld metal regions. Intensive mixing of the base, filler and insert materials led to formation of microregions of different etchability through the entire volume of the weld with different concentration of alloying elements (Figure 5, *a*). However, standard optical metallography methods did not allow revealing any morphological signs of primary structure recrystallization products. Contrarily, the results of studying the Mars 600

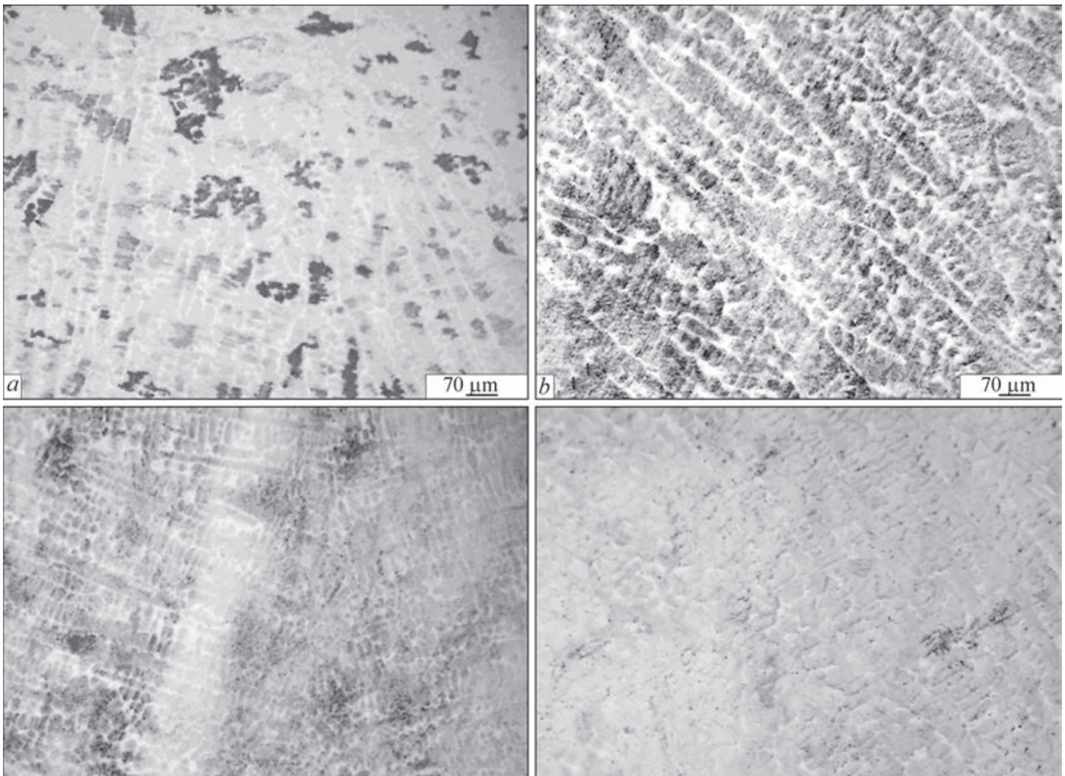

**Figure 5.** Microstructure of weld metal of the welded joints (×200): Armox 500T steel (*a*) and Mars 600 steel — root region (*b*), middle region (*c*), upper region (*d*)

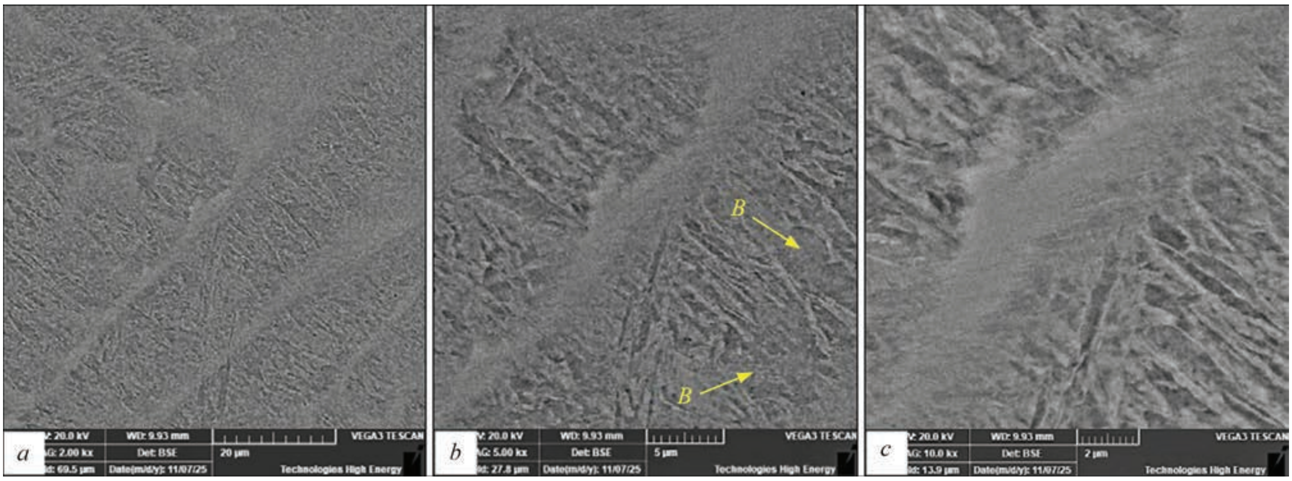


**Figure 6.** Microstructure of weld metal of Armox 500T steel sample: ×2000 (*a*); ×5000 (*b*); ×10000 (*c*). B — bainite of block morphology

steel sample point to formation of a heterogeneous (at the macrolevel) structure of the weld, which correlates with the determined microhardness distribution along its vertical axis (Figure 2). Lath martensitic structure was detected inside the crystallites of the weld metal root area (Figure 5, *b*). Within the middle weld region along the height, which features a reduction of microhardness, optical microscopy did not detect any martensite packets, but light-etching bands appeared (Figure 5, *c*). The upper region of the weld, where the metal has somewhat higher microhardness values, looks like a solid "white layer", where just the dendritic crystallite boundaries are etched (Figure 5, *d*).

The features of structure formation in the weld determined for Mars 600 steel sample are due to its more intensive alloying by welding consumables, compared to the weld on Armox 500T steel sample, owing to a higher filler wire feed rate, larger diameter of the insert rod and lower welding speed.

Scanning electron microscopy revealed the martensitic-bainitic structure of the weld metal of the welded sample from Armox 500T steel. Lath martensite packets (Figure 6, *a*, *c*), as well as bainitic structure blocks (Figure 6, *b*), are present within the individual branches of the columnar crystallites. Their formation is caused by the concentration heterogeneity of the alloying element distribution in the weld metal. The average width of the columnar crystallites is equal to 13–22 μm.

The structure of cast metal in the root area of the weld of Mars 600 steel welded sample is homogeneous, fine-acicular martensitic (Figure 7, *a*–*c*). The average width of the columnar crystallites reaches 14–30 μm. Contrarily, the metal of the weld upper region has a much finer primary structure with the crystallite width of 5–12 μm (Figure 7, *d*–*f*), which is, obviously, due to the features of the influence of the pulsating constricted arc on the weld pool solidification conditions, simultaneously alloyed by the filler and insert wires. No acicular or packet structure of classical martensite was found inside the dendrite cells even with the magnification of ×10000 (Figure 7, *e*).

The high microhardness of ~580–600 $HV_{0.3}$ in the metal of the weld upper region determined in the Mars 600 steel sample (Figure 2) and the results of microstructural studies (Figure 5, *d*; Figure 7, *f*) are indicative of formation in this part of the weld of the so-called structureless martensite (hardenite) — a nanocrystalline mixture of martensite and residual austenite. The **"**white layer**"** of structureless martensite, created by the methods of hardening treatment of the surface of the engineering and tool steels [26, 27], as well as heterogeneous steel armor [28], is characterized by a high hardness and friction and wear resistance. Refinement of the dendritic structure in the weld upper region due to intensive mixing of the pool melt, with further overcooling below $M_s$ temperature promoted blocking of martensite crystals growth by the boundaries of highly refined austenite grains, that, according to the classical concepts [29], is the necessary precondition of structureless martensite formation.

Results of studying the chemical composition of weld regions in joints of Armox 500T and Mars 600 steels are given in Table 3. Considering the high error of EDX-determination of carbon concentration, its average content in the metal of both the welds was determined additionally by the method of NDIR-spectroscopy. One can see from the data in Table 3 that the average carbon content in the weld metal of Armox 500T steel sample almost did not decrease compared to its content in the base metal (Table 1). At the same time, the average carbon content in the weld metal of the Mars 600 steel sample was reduced by ~25 % compared with the base metal. For welds of the joints of both the steels, there is a tendency toward a reduction of the content of all the alloying elements alongside an increase in the carbon concentration in the weld root

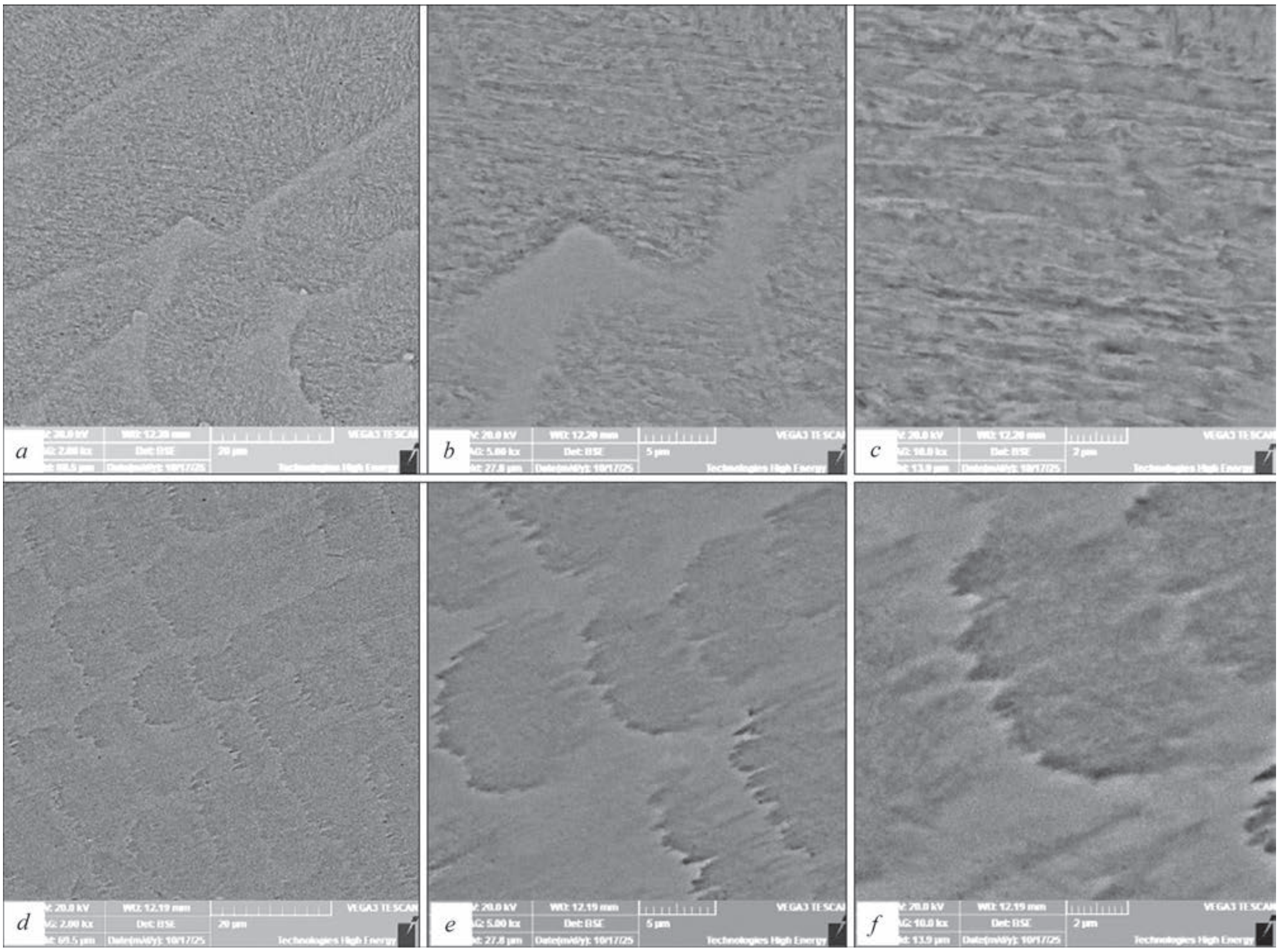


**Figure 7.** Microstructure of the root (*a–b*) and upper (*d–f*) regions of weld metal of Mars 600 steel sample: ×2000 (*a*, *d*); ×5000 (*b*, *e*); ×10000 (*c*, *f*)

regions, compared with the upper regions, despite the near-root position of the low-carbon high-alloy insert material. This effect is attributable to the features of the pulsating constricted arc influence on the hydrodynamic and convective fluxes in the pool melt.

Despite the presence of signs of structureless martensite in the metal of upper region of the weld on the Mars 600 steel, it is somewhat inferior to the hardness values for the root region metal (Figure 2), because of the significantly lower carbon content. Moreover, this is the only region of all the studied regions of both the welds, where the total alloying element content meets the criteria for high-alloy steel (>10 wt.%).

Results of ballistic tests of the welded samples are given in Figure 8. According to the test protocol, a sample from Armox 500T steel 5.4 mm thick has passed ballistic tests for resistance to fire from a 5.45×39 mm 7N6M assault rifle cartridge with a PS bullet (a bul-

**Table 3.** Chemical composition of weld metal of the studied welded joints, wt.%

| Method of analysis | Element | Armox 500T | | Mars 600 | | |
|---|---|---|---|---|---|---|
| | | Weld region | | Weld region | | |
| | | Top | Root | Top | Middle | Root |
| EDX | C | 6.04* | 6.54* | 6.81* | 7.60* | 8.42* |
| | Si | 0.26 | 0.20 | 0.65 | 0.62 | 0.58 |
| | Mn | 1.60 | 1.49 | 1.81 | 1.30 | 1.20 |
| | Cr | 4.56 | 2.96 | 5.10 | 3.79 | 3.63 |
| | Ni | 1.94 | 1.79 | 3.30 | 2.88 | 2.69 |
| | Mo | 0.28 | 0.26 | 0.24 | 0.20 | 0.21 |
| NDIR | C | 0.27 | | 0.32 | | |

*Due to the high measurement error, the carbon content values determined by the method of energy-dispersive X-ray spectroscopy, are given only for comparative analysis.

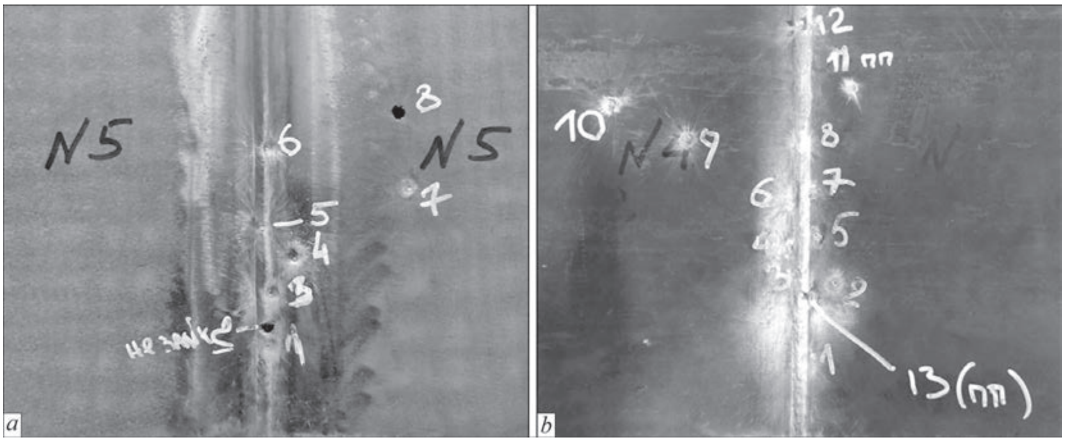


**Figure 8.** Appearance of welded samples after ballistic testing: *a* — Armox 500T steel; *b* — Mars 600 steel

let with a hardened steel core in a steel jacket), which is defined as protection class PZSA-3, according to DSTU 3975–2000. Shooting of the sample using the 7N10 cartridge with a PP bullet (an enhanced-penetration bullet with a hardened steel core in a steel jacket) caused complete penetration (Figure 8, *a*) both in the weld metal (hit No. 2, “fail”) and in the base metal unaffected by the welding thermal cycle (hit No. 8).

A welded sample made of Mars 600 steel 6.2 mm thick, successfully withstood ballistic testing for resistance to impacts from both types of ammunition (Figure 8, *b*): the PS bullet (hits Nos 1–9), as well as the PP bullet (hits Nos 10–13), which meets the requirements of the PZSA-4 protection class in accordance with the DSTU 3975-2000 standard.

## DISCUSSION OF RESULTS

Obtained results show that application of pulsed-plasma welding with combined alloying of the weld metal allows realizing an approach to armor steel welding with application of high-alloy austenitic filler materials, which differs significantly from the traditional technologies of mechanized arc welding. The latter are characterized by formation of an austenitic or austenitic-ferritic weld metal with the hardness level lower than that of the base metal, which is often regarded as one of the factors reducing the local ballistic resistance of armor steel welded joints.

In the studied joints a different approach to formation of the weld metal structure and properties is realized. Martensitic-type structures form in the weld metal, despite the application of high-alloy welding consumables of austenitic class. This is indicative of the important role of the base metal in formation of the weld structure and confirms the effectiveness of combined alloying application under the conditions of a high proportion of the base metal in the weld metal.

Comparison of the results for Armox 500T and Mars 600 steels showed that the pattern of structure formation is determined not only by the welding conditions, but also by the features of armor steel chemical composition. A higher carbon and silicon content in Mars 600 steel favours the formation of finer martensitic structures and improves the metal resistance to the tempering processes in the HAZ. This is in agreement with the microhardness measurement results and the determined reduction in the width of the HAZ softened zone, compared to Armox 500T steel.

One of the key features of the applied technology is application of the pulsed mode of plasma welding. It is known that the periodical change in the plasma arc current is accompanied by a change in the current density, electromagnetic forces, degree of the arc constriction, and pressure of the plasma flux on the melt surface, which results in appearance of the nonstationary convective fluxes in the weld pool and intensification of mass transfer in the melt [14–16].

In keeping with the data of [14], the surface tension forces, electromagnetic forces, plasma flux and buoyancy forces have the decisive influence on the metal flow in plasma welding. When operating in the pulsed mode, the above factors act in the nonstationary mode, leading to a periodical disturbance of the melt and intensification of the mass transfer processes. Similar tendencies as to the influence of the pulsed arc on weld formation, structure refinement and increase of the metal homogeneity were also established in [13, 15, 16].

Taking into account the derived results, it can be assumed that the determined features of alloying element and carbon distribution along the weld height, as well as formation of a heterogeneous weld metal structure are the result of the combined action of alloying and intensive stirring of the weld pool metal. The periodical change in the pressure of the plasma flux and the electromagnetic forces may promote a more effective interaction of the base metal with the filler wire and the insert rod, creating the conditions for formation of a gradient distribution of the chemical elements in the weld metal.

An important feature of the obtained results is the fact that the high ballistic resistance of the welded joints is achieved not due to the local strengthening of individual regions, but as a result of formation of a more balanced structural and mechanical state of the welded joint as a whole. Formation of high-strength weld metal of martensitic type in a combination with the restricted width of the softened HAZ regions allows avoiding an abrupt mismatch in the properties between the individual joint zones, which is one of the key factors for ensuring the ballistic resistance at the base metal level.

Thus, investigation results indicate that application of pulsed-plasma welding with combined alloying of the weld metal creates the conditions for formation of a martensitic-type weld metal with the ballistic resistance level equivalent to that of the base metal in the heat-hardened condition. Achievement of such a result is due to the combined action of the high proportion of the base metal in the weld metal, combined alloying with filler wire and insert rod of austenitic class, as well as the features of the hydrodynamic processes in the weld pool in the pulse mode of plasma welding. It is probable that the periodical action of the pulsating constricted plasma arc promotes an intensification of mass transfer and mixing of the melt, creating additional preconditions for formation of the established structural state of the weld metal [14–16].

## CONCLUSIONS

1. It is shown that pulsed-plasma welding with independent regulation of the heat input and filler metal quantity ensures formation of full-penetration butt joints of Armox 500T and Mars 600 armor steels 5–6 mm thick without edge preparation at the specific heat input of $Q/\delta \approx 0.16$ kJ/mm$^2$. At the same level of thermal impact, Mars 600 steel features a smaller width of the HAZ softened region, compared with Armox 500T steel, which is associated with an increased silicon content and higher resistance of its martensitic structure to short-time tempering.

2. It was determined that combined alloying of the weld metal with OK Autrod 16.95 filler wire and OK Tigrod 308L insert rod in combination with a high proportion of the base metal in the weld allows avoiding the formation of a soft austenitic weld metal, characteristic for the traditional MAG-welding of armor steels. A martensitic-bainitic structure of the weld metal forms in the joints of Armox 500T steel with a hardness, which is not inferior to base metal hardness.

3. For Mars 600 steel a pronounced structural anisotropy of the weld metal along its height was found. In the root region a fine-acicular martensite with the highest microhardness value is formed, in the middle part — a structure with lower hardness values, and in the upper region — a refined structure with the signs of structureless martensite. The derived results are indicative of a significant influence of the solidification conditions and alloying element distribution on the weld metal structure formation.

4. It is shown that application of the pulsed mode of plasma welding is one of the important features of the used technology. Taking into account the results of structural and chemical studies it can be assumed that the periodical action of the pulsating constricted plasma arc promotes an intensification of mass transfer and mixing of the weld pool metal, creating additional prerequisites for formation of a graded distribution of alloying elements and carbon along the weld height.

5. Ballistic testing confirmed that the developed technology of plasma-arc welding with combined alloying of the weld metal ensures producing welded joints of armor steels of different hardness classes, with ballistic resistance equivalent to that of the base metal. For samples from Mars 600 steel, resistance to impacts from PS and PP bullets is ensured, whereas for Armox 500T it has been established that destruction is determined by the bullet resistance level of the base metal under stricter testing conditions, rather than by the properties of the weld.

## REFERENCES

1. DSTU V 9014:2020: *Arc welding of high-hardness steel structures for light armored vehicles. Technical specifications*. Kyiv, SE “UkrNDNTs” [in Ukrainian].
2. Men, I., Naroditsky, D. (2023) Vibration fatigue testing procedure of high strength MARS 600 steel fillet welds using stainless steel consumable electrode. *Advanced Engineering Forum,* **49**, 57–78. DOI: https://doi.org/10.4028/p-o0a804
3. Gaivoronskyi, O.A., Poznyakov, V.D., Zavdoveyev, A.V. et al. (2023) Prevention of cold cracking in armour steel welding. *The Paton Welding J.*, **5**, 3–10. DOI: https://doi.org/10.37434/tpwj2023.05.01
4. Çoban, O., Kaymak, F., Gürol, U. et al. (2025) Characterization of fillet welded armor steel performed by robotic gas metal arc welding: effect of heat input on microstructure and microhardness. *J. of Mater. Eng. and Perform.*, **34**, 231–244. DOI: https://doi.org/10.1007/s11665-023-09058-y
5. Slyvinskyy, O.A., Kvasnytskyi, V.V., Prokhorenko, O.V. et al. (2025) The influence of low-temperature austenite transformation in weld metal on the residual stress state of welded joints of armor steel. *Metallofiz. Noveishie Tekhnol.*, **47**, 1295–1318 [in Ukrainian]. DOI: https://doi.org/10.15407/mfint.47.12.1295
6. Madhusudhan Reddy, G., Mohandas, T., Papukutty, K.K. (1998) Effect of welding process on the ballistic performance of high-strength low-alloy steel weldments. *J. Mater. Process Tech.*, 74(**1–3**), 27–35. DOI: https://doi.org/10.1016/S0924-0136(97)00245-8
7. Slyvinskyy, O.A., Kovtoniuk, M.M. (2025) Approaches to enhancing the ballistic performance of welded joints in high and ultra-high hardness armor steels (Review). *The Paton Welding J.*, **12**, 11–19. DOI: https://doi.org/10.37434/tpwj2025.12.02
8. Morsy, M.A., Abdel Aziz, S.M., Abdelwahed, K. et al. (2022) Effect of welding parameters on the mechanical and metallur-

gical properties of armor steel weldment. *J. Eng. Appl. Sci.*, **69**, 62. DOI: https://doi.org/10.1186/s44147-022-00102-7
9. Sowards, J.W., Hussey, D.S., Jacobson, D.L. et al. (2018) Correlation of neutron-based strain imaging and mechanical behavior of armor steel welds produced with the hybrid laser arc welding process. *J. Res. Natl. Inst. Stand. Technol.*, **123**, 123011. DOI: https://doi.org/10.6028/jres.123.011
10. Günena, A., Bayara, S., Karakaş, M.S. (2020) Effect of different arc welding processes on the metallurgical and mechanical properties of Ramor 500 armor steel. *J. Eng. Mater. Technol.*, **142**, 021007. DOI: https://doi.org/10.1115/1.4045569
11. Skowrońska, B., Szulc, J., Bober, M. et al. (2022) Selected properties of Ramor 500 steel welded joints by hybrid PTA-MAG. *J. Adv. Join. Proces.*, **5**, 100111. DOI: https://doi.org/10.1016/j.jajp.2022.100111
12. Son, H.J., Jeong, Y.C., Seo, B.W. et al. (2023) Weld quality analysis of high-hardness armored steel in pulsed gas metal arc welding. *Metals*, 13(**2**), 303. DOI: https://doi.org/10.3390/met13020303
13. Sathish Kumar, K., Arivazhagan, N. (2024) An innovative pulsed current arc welding technology for armor steel: Processes, microstructure and mechanical properties. *Mater. Today Commun*., **38**, 108237. DOI: https://doi.org/10.1016/j.mtcomm.2024.108237
14. Ngo Huu, M., Nguyen Van, A., Nguyen Van, T. et al. (2020) Material flow behavior on weld pool surface in plasma arc welding process considering dominant driving forces. *Appl. Sci.*, 10(**10**), 3569. DOI: https://doi.org/10.3390/app10103569
15. Lu, Z., Zhang, W., Jiang, F. et al. (2019). A primary study of variable polarity plasma arc welding using a pulsed plasma gas. *Materials*, 12(**10**), 1666. DOI: https://doi.org/10.3390/ma12101666
16. Wang, Z., Jiang, D., Wu, J., Xu, M. (2020) A review on high-frequency pulsed arc welding. *J. Manuf. Process*., **60**, 503–519. DOI: https://doi.org/10.1016/j.jmapro.2020.10.054
17. (2008) MIL-DTL-46100E (MR) with Amendment 1. *Armor plate, steel, wrought, high hardness.* U.S. Detail Specification. Aberdeen, U.S. Army Research Laboratory.
18. MIL-DTL-32332A (MR). *Armor plate, steel, wrought, ultra-high hardness* (2018) U.S. Detail Specification. Aberdeen, U.S. Army Research Laboratory.
19. Khoshnaw, F., Krivtsun, I., Korzhyk, V. (2023) Chapter 2. Arc welding methods. In: *Welding of metallic materials: Methods, metallurgy and performance.* Ed. by F. Khoshnaw. Amsterdam, Elsevier, 37–71. DOI: https://doi.org/10.1016/B978-0-323-90552-7.00004-3
20. Sydorets, V., Korzhyk, V., Khaskin, V. et al. (2017) Electrical characteristics of the equipment for the hybrid plasma-MIG welding. In: *Proc. of the IEEE 58th Inter. Scientific Conf. on Power and Electrical Engineering of Riga Technical University (RTUCON), Riga, Latvia*, 1–6. DOI: https://doi.org/10.1109/RTUCON.2017.8124811
21. Kvasnytskyi, V., Korzhyk, V., Lahodzinskyi, I. et al. (2020) Creation of volumetric products using additive arc cladding with compact and powder filler materials. In: *Proc. of IEEE 10th Inter. Conf. Nanomaterials: Applications & Properties (NAP), Sumy, Ukraine,* 02SAMA16-1–02SAMA16-5. DOI: https://doi.org/10.1109/NAP51477.2020.9309696
22. Shevchenko, V., Korzhyk, V., Gao, S. et al. (2024) Formation of stainless steel welded joints produced with the application of laser and plasma energy sources. *Metals*, 14(**6**), 706. DOI: https://doi.org/10.3390/met14060706
23. Garasym, Ju. A., Bondarevska, N.O., Teliovich, R.V. et al. (2021) Influence of high-speed heat-setting on armor resistance of high-strength sheet metal of protective purpose. *Metallofiz. Noveishie Tekhnol.*, **43**, 1235–1246 [in Ukrainian]. DOI: https://doi.org/10.15407/mfint.43.09.1235
24. Wang, Lj., Cai, Qw., Wu, Hb. et al. (2011) Effects of Si on the stability of retained austenite and temper embrittlement of ultrahigh strength steels. *Inter. J. Miner. Metall. Mater.*, **18**, 543–550. DOI: https://doi.org/10.1007/s12613-011-0475-0
25. Kim, B., Celada, C., San Martín, D. et al. (2013) The effect of silicon on the nanoprecipitation of cementite. *Acta Mater.*, **61**, 6983–6992. DOI: https://doi.org/10.1016/j.actamat.2013.08.012
26. Kozechko, V.A., Kozechko, V.I. (2024) Combined ultrasonic-mechanical treatment. *Metallofiz. Noveishie Tekhnol.*, **46**, 851–860. DOI: https://doi.org/10.15407/mfint.46.09.0851
27. Kolisnichenko, O.V., Korzhyk, V.M., Senderowski, C. et al. (2025) Influence of pulse plasma treatment on wear resistance of 40Kh steel surface layers. *The Paton Welding J.*, **9**, 39–45. DOI: https://doi.org/10.37434/tpwj2025.09.05
28. Bolotsky, M. (1945) *Armor-rolled: Metallurgical examination of British homogenous and face hardened armor*. Technical report WAL 710/724. Watertown Arsenal Laboratory.
29. Zav'yalov, A.S., Teplukhin, G.N., Gabeev, K.V. (1979) Conditions and mechanism of formation of structureless martensite (hardenite). *Met. Sci. Heat Treat*., **21**, 750–752. DOI: https://doi.org/10.1007/BF00708376

**ORCID**

O.A. Slyvinskyy: 0000-0001-6418-4898,
V.D. Poznyakov: 0000-0001-8581-3526,
V.M. Korzhyk: 0000-0001-9106-8593,
Ye.V. Illiashenko: 0000-0001-9876-0320,
S.P. Bisyk: 0000-0002-5009-2113

**CONFLICT OF INTEREST**

The Authors declare no conflict of interest

**CORRESPONDING AUTHOR**

O.A. Slyvinskyy
[1]National Technical University of Ukraine
"Igor Sikorsky Kyiv Polytechnic Institute"
37 Prosp. Beresteiskyi, 03056, Kyiv, Ukraine.
[2]E.O. Paton Electric Welding Institute of the NASU
11 Kazymyr Malevych Str., 03150, Kyiv, Ukraine
E-mail: o.slyvinsky@gmail.com

**SUGGESTED CITATION**

O.A. Slyvinskyy, V.D. Poznyakov, V.M. Korzhyk, Ye.V. Illiashenko, S.P. Bisyk (2026) Features of formation of the structure and ballistic resistance of armor steel welded joints produced by pulsed plasma arc welding with combined alloying of the weld metal. *The Paton Welding J*., **08**, 3–12.
DOI: https://doi.org/10.37434/tpwj2026.08.01

**JOURNAL HOME PAGE**

https://patonpublishinghouse.com/eng/journals/tpwj

Received: 30.04.2026
Received in revised form: 16.06.2026
Accepted: 27.07.2026